Electronic Supplementary Material (ESI) for Inorganic Chemistry Frontiers.

Supporting Information

Multifunctional protective layer filled with 2D anionic nanosheets enabling dendrite-free zinc anode

Sangsang Liu,[a,b] Qin Yu,[a,b] Haitao Liu,[a,b] Wenlong Chen,[a,b] Fugang Qi,[a,b,*] Yilong Dai,[a,b] Yaru Liang,[a,b,*] Weihong Lai,[c,*] Xiaoping Ouyang[a,b]

[a] School of Materials Science and Engineering, Xiangtan University, Xiangtan 411105, P. R. China

[b] Key Laboratory of Low Dimensional Materials and Application Technology of Ministry of Education, Xiangtan University, Xiangtan 411105, P. R. China

[c] Institute for Superconducting and Electronic Materials, Australian Institute of Innovative Materials, Innovation Campus, University of Wollongong, Wollongong, NSW 2500, Australia

*E-mail(Corresponding author): yaruliang@xtu.edu.cn (Yaru Liang)

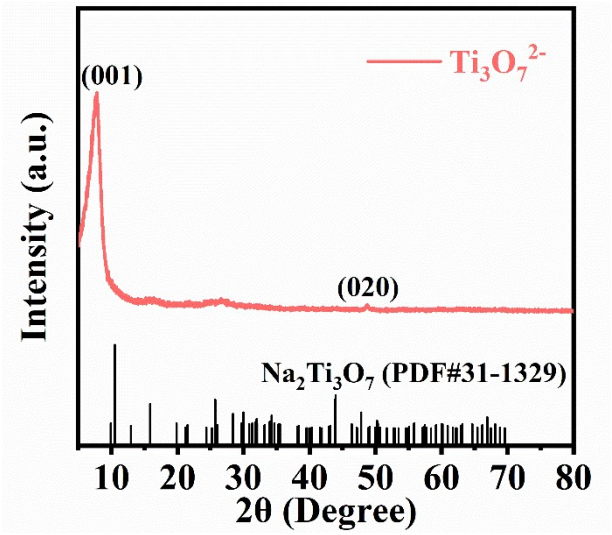

Fig. S1 XRD pattern of $Ti_3O_7^{2-}$ nanosheets.

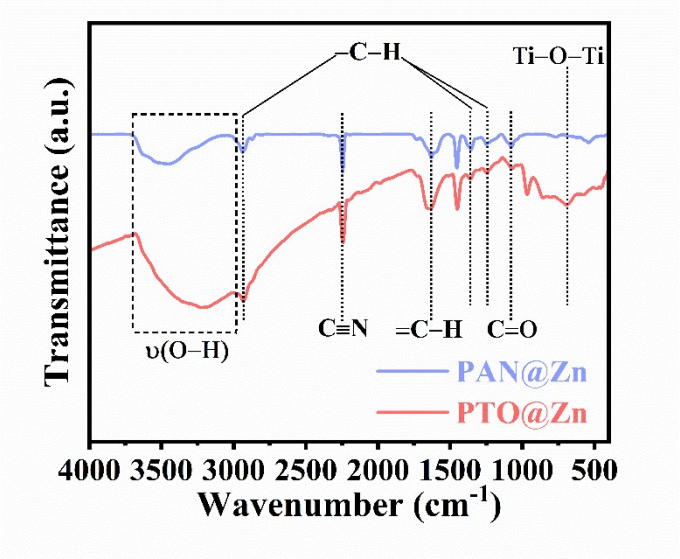

Fig. S2 FTIR spectrum of PAN@Zn and PTO@Zn.

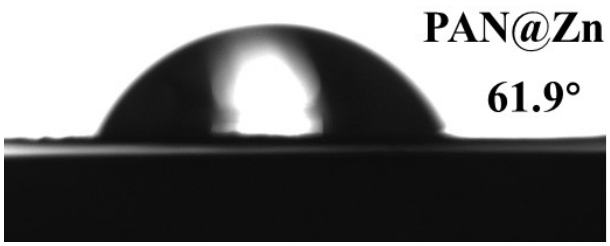

Fig. S3 Contact angles of PAN@Zn electrode.

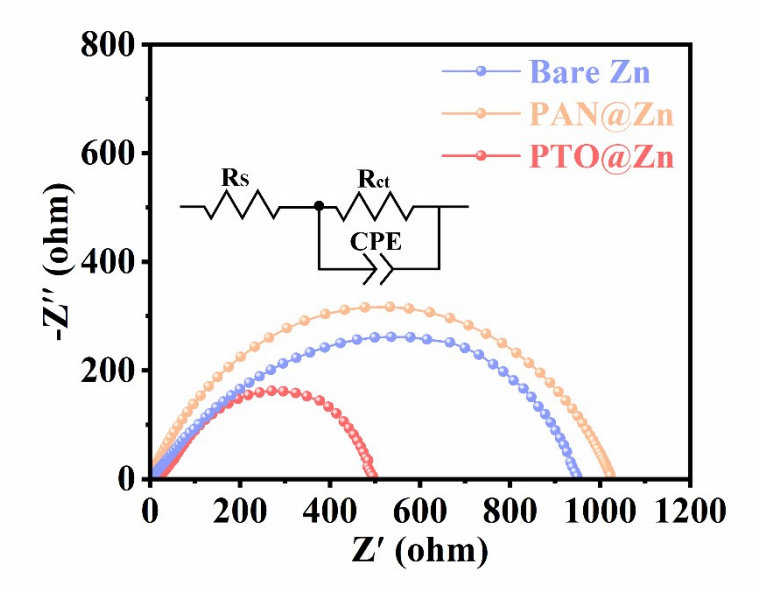

Fig. S4 EIS spectra of the bare Zn, PAN@Zn and PTO@Zn symmetric cells.

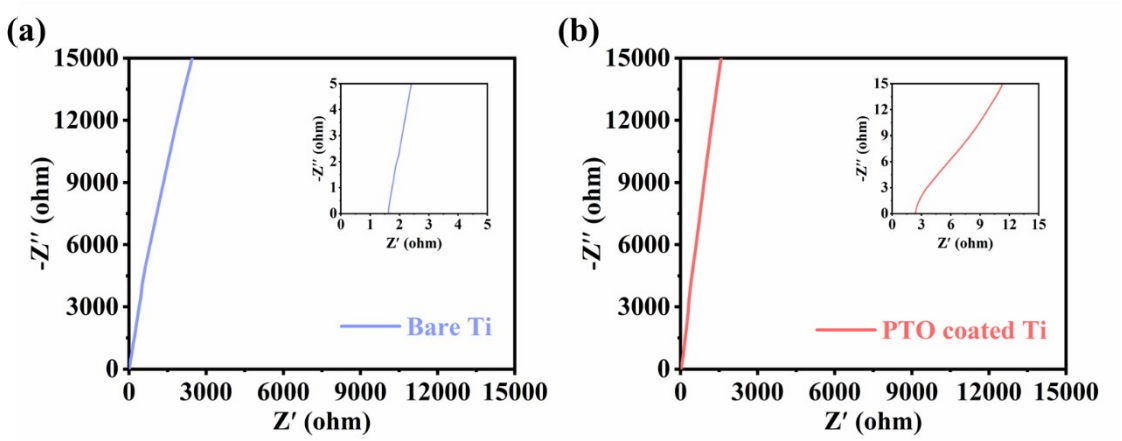

Fig. S5 Nyquist plots over the frequency range of 100 kHz to 10 mHz of (a) the symmetrical cell with Ti as electrodes and (b) the symmetrical cell with PTO-coated Ti as electrodes (inset: enlargement of indicated range). The ionic conductivity (σ) is calculated according to the following equation,

$$\sigma = \frac{L}{R_b \cdot S}$$

where L is the thickness of the PTO layer, R_b is the bulk impedance of the PTO layer, and S is the contact area.

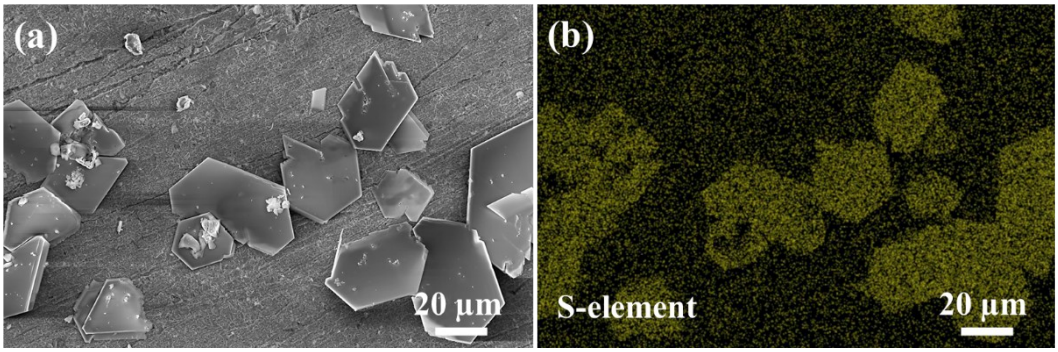

Fig. S6 (a) SEM image and (b) corresponding EDS mapping of S element of the Zn foil after being soaked in 2 M $ZnSO_4$ for 10 days.

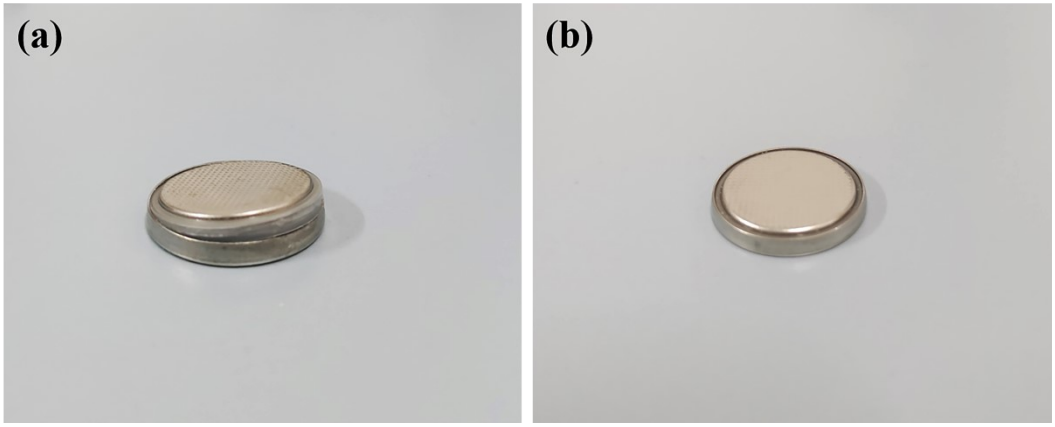

Fig. S7 Photographs of (a) bare Zn and (b) PTO@Zn symmetrical battery after stripping/plating.

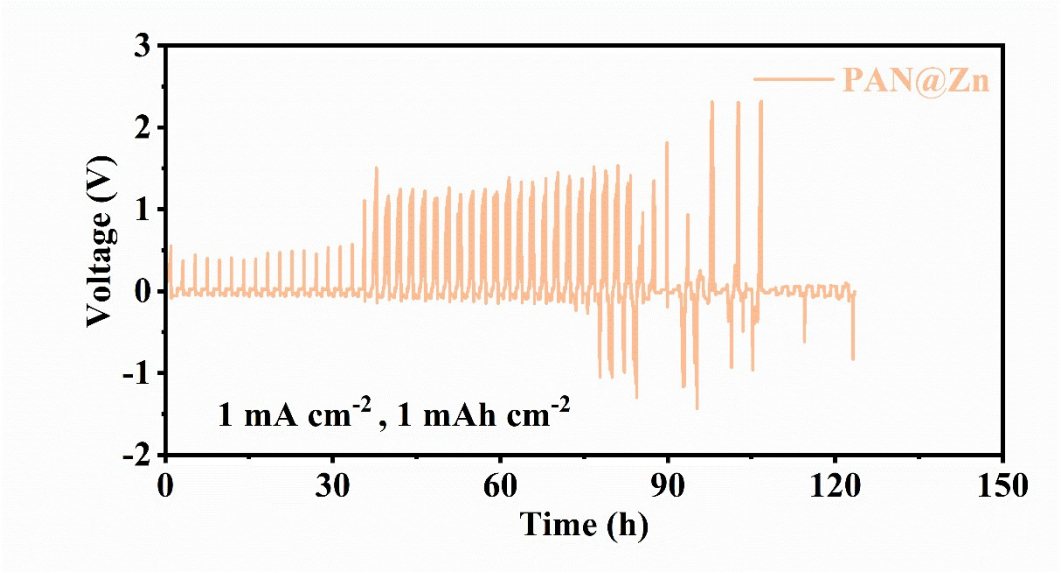

Fig. S8 Cycling performance of symmetrical PAN@Zn||PAN@Zn cell at 1 mA cm^{-2} with a capacity of 1 mAh cm^{-2}.

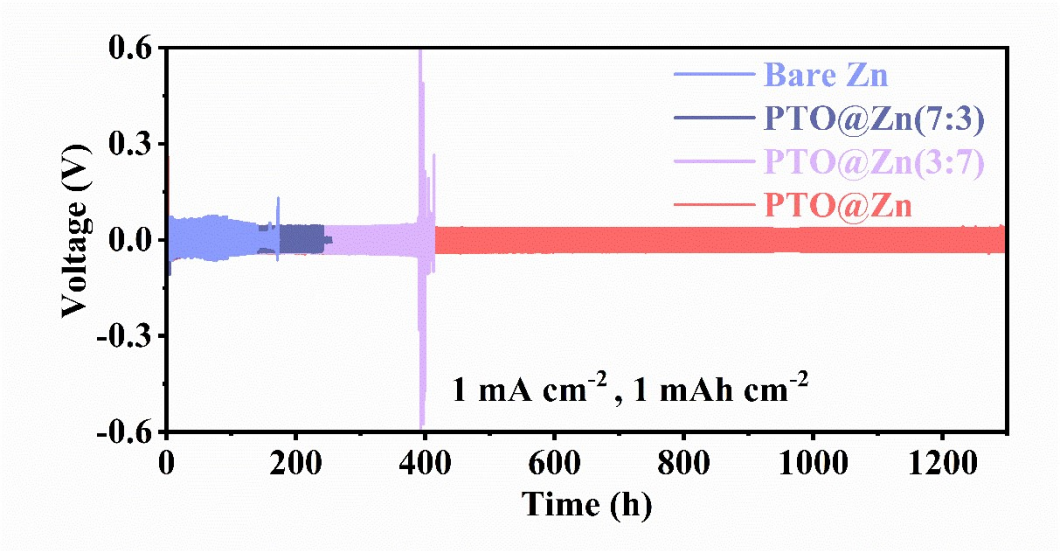

Fig. S9 Cycling performance of symmetrical Zn||Zn and PTO@Zn||PTO@Zn cells at 1 mA cm^{-2} with a capacity of 1 mAh cm^{-2}. The PTO coating layers have different mass ratios of PTO and 2D $Ti_3O_7^{2-}$ nanosheets. For the layers with m(PAN):m($Ti_3O_7^{2-}$) ratios of 1:1, 7:3 and 3:7, the electrodes are donated as PTO@Zn, PTO@Zn(7:3), and PTO@Zn(3:7), respectively.

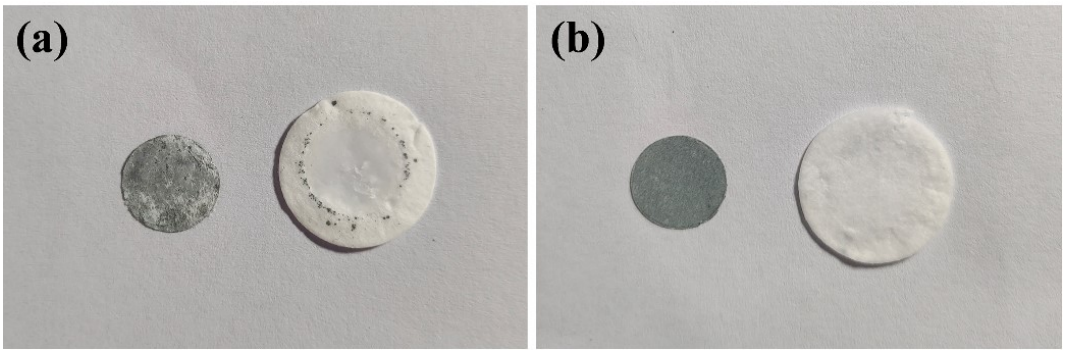

Fig. S10 Digital images of the electrodes and separators disassembled from the (a) bare Zn and (b) PTO@Zn symmetric cells after 20 cycles at 5 mA cm^{-2}/5 mAh cm^{-2}.

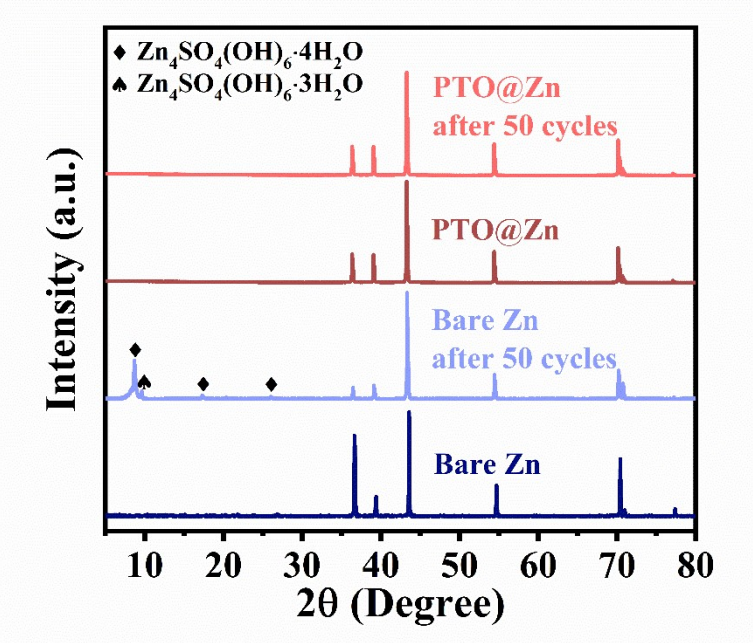

Fig. S11 The XRD patterns of the bare Zn and PTO@Zn before and after cycling.

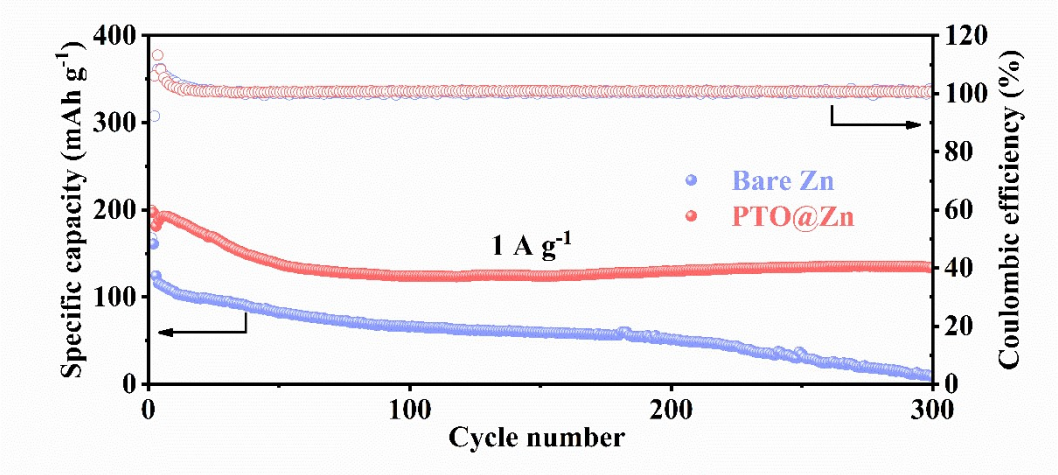

Fig. S12 Cycling performance of Zn||MnO_2 and PTO@Zn||MnO_2 cells under low N/P ratio cycled at 1 A g^{-1}.

Table S1. Comparison of cycling performance for this work with recently reported Zn-based Zn||MnO_2 full cells.

Anode (Thickness, μm)	Cathode mass loading (mg cm^{-2})	N/P ratio	Current density	Specific capacity (mAh g^{-1})	Reference
$Zn_{0.73}Al_{0.27}$@Zn (200)	2.0	~63	1.2 C (1C = 616 mA g^{-1})	~243	1
Zn|Sn (20)	1.2	~33	1 A g^{-1}	124	2
Zn|Sn (250)	15.8	~31	0.2 A g^{-1}	92	
Zn@MCFs (100)	1.0	/	1 A g^{-1}	236.1	3
AEC-Zn (80)	1.0	/	2 C (1 C=308 mA g^{-1})	244	4
Cu@Zn (40)	1.5	/	1 A g^{-1}	~120	5
PA-Zn (20)	~1.3	/	2 C (1 C=300 mA g^{-1})	176.1	6
	~15	/		175	
ZnS@Zn (10)	~0.8	/	5 C (1 C=308 mA g^{-1})	125.8	7
Zn-VSGDY (10)	1.3-2.6	/	1 A g^{-1}	125.4	8
PTO@Zn (30)	1.0-1.2	~47	1 A g^{-1}	198.6	This work
PTO@Zn (10)	~2.1	~9		196.8	

Reference

1 J. Zheng, Z. Huang, Y. Zeng, W. Liu, B. Wei, Z. Qi, Z. Wang, C. Xia and H. Liang, Electrostatic Shielding Regulation of Magnetron Sputtered Al-Based Alloy Protective Coatings Enables Highly Reversible Zinc Anodes, *Nano Lett.*, 2022, **22**, 1017–1023.

2 P. Xiong, Y. Kang, H. Yuan, Q. Liu, S. H. Baek, J. M. Park, Q. Dou, X. Han, W.-S. Jang, S. J. Kwon, Y.-M. Kim, W. Li and H. S. Park, Galvanically replaced artificial interfacial layer for highly reversible zinc metal anodes, *Appl. Phys. Rev.*, 2022, **9**, 011401.

3 H. Ying, P. Huang, Z. Zhang, S. Zhang, Q. Han, Z. Zhang, J. Wang and W. Q. Han, Freestanding and Flexible Interfacial Layer Enables Bottom-Up Zn Deposition Toward Dendrite-Free Aqueous Zn-Ion Batteries, *Nano-Micro Lett.*, 2022, **14**, 180.

4 R. Zhao, Y. Yang, G. Liu, R. Zhu, J. Huang, Z. Chen, Z. Gao, X. Chen and L. Qie, Redirected Zn Electrodeposition by an Anti-Corrosion Elastic Constraint for Highly Reversible Zn Anodes, *Adv. Funct. Mater.*, 2020, **31**, 2001867.

5 Y. Zhang, G. Wang, F. Yu, G. Xu, Z. Li, M. Zhu, Z. Yue, M. Wu, H.-K. Liu, S.-X. Dou and C. Wu, Highly reversible and dendrite-free Zn electrodeposition enabled by a thin metallic interfacial layer in aqueous batteries, *Chem Eng J*, 2021, **416**, 128062.

6 Z. Zhao, J. Zhao, Z. Hu, J. Li, J. Li, Y. Zhang, C. Wang and G. Cui, Long-life and deeply rechargeable aqueous Zn anodes enabled by a multifunctional brightener-inspired interphase, *Energy Environ. Sci.*, 2019, **12**, 1938-1949.

7 J. Hao, B. Li, X. Li, X. Zeng, S. Zhang, F. Yang, S. Liu, D. Li, C. Wu and Z. Guo, An In-Depth Study of Zn Metal Surface Chemistry for Advanced Aqueous Zn-Ion Batteries, *Adv Mater*, 2020, **32**, e2003021.

8 X. Liu, K. Wang, Y. Liu, F. Zhao, J. He, H. Wu, J. Wu, H. P. Liang and C. Huang, Constructing an ion-oriented channel on a zinc electrode through surface engineering, *Carbon Energy*, 2023, e343.